Ground and excited states of even-numbered Hubbard ring at half-filling: comparison of the extended Gutzwiller approach with exact diagonalization

Ground and excited states of even-numbered Hubbard ring at half-filling: comparison of the extended Gutzwiller approach with exact diagonalization

Yimei Fang,[1] Feng Zhang,[2,3,*] Zhuo Ye,[2] Han Zhang,[4] Wen-Cai Lu,[4] Shunqing Wu,[1,†] Yong-Xin Yao,[2,3] Cai-Zhuang Wang,[2,3] Kai-Ming Ho[3]

[1]Department of Physics, OSED,
Key Laboratory of Low Dimensional Condensed Matter Physics
(Department of Education of Fujian Province)
Jiujiang Research institute, Xiamen University, Xiamen 361005, China.
[2]Division of Materials Science and Engineering, Ames National Laboratory, Ames, Iowa 50011, United States
[3]Department of Physics, Iowa State University, Ames, Iowa 50011, United States
[4]College of Physics, Qingdao University, Qingdao, Shandong 266071, China

E-mail: *fzhang@ameslab.edu

E-mail: †wsq@xmu.edu.cn

Abstract. It remains a great challenge in condensed matter physics to develop a method to treat strongly correlated many-body systems with balanced accuracy and efficiency. We introduce an extended Gutzwiller (EG) method incorporating a manifold technique, which builds an effective manifold of the many-body Hilbert space, to describe the ground- and excited-state properties of strongly correlated electrons. We systematically apply an EG projector onto the ground and excited states of a non-interacting system. Diagonalization of the true Hamiltonian within the manifold formed by the resulting EG wavefunctions gives the approximate ground and excited states of the correlated system. To validate this technique, we implement it on even-numbered fermionic Hubbard rings at half-filling with periodic boundary conditions, and compare the results with the exact diagonalization (ED) method. The EG method is capable of generating high-quality ground and low-lying excited state wavefunctions, as evidenced by the high overlaps of wavefunctions between the EG and ED methods. Favorable comparisons are also achieved for other quantities including the total energy, the double occupancy, the total spin and the staggered magnetization. With the capability of accessing the excited states, the EG method can capture the essential features of the one-electron removal spectral function that contains contributions from states deep in the excited spectrum. Finally, we provide an outlook on the application of this method on large extended systems.

Keywords: correlated electron systems, extended Gutzwiller, Hubbard ring, spectral function

1. Introduction

Despite its simple format, the Hubbard model [1] has received a steady stream of attention since it is able to capture a variety of important physics of strongly correlated systems in real materials, such as spin-charge separation in $SrCuO_2$ [2], and high-temperature superconductivity in cuprates [3]. Early in 1960s, Lieb and Wu provided an exact solution of the one-dimensional (1D) single-band Hubbard model using the Bethe ansatz equations [4]. However, the exact solution at 2D and 3D, or even 1D multiple-band system would be extremely difficult or even impossible due to the exponential scaling of computational resources required for exact calculations [5].

Truncation or variational methods [6] are used to obtain numerical solutions that cover situations where exact solutions are not known. A variety of numerical methods have emerged as reliable solutions to study the Hubbard models. For example, the quantum Monte Carlo (QMC) method [7, 8], the density matrix renormalization group (DMRG) scheme [9–11], the dynamical variational principle [12, 13], and the symmetry-projected variational approach [6]. Our previously developed Gutzwiller conjugate gradient minimisation theory (GCGM) [14, 15] constitutes another efficient approach for describing strongly correlated electron systems, which has proved to provide satisfying accuracy of the ground-state energy and wavefunction of 1D and 2D Hubbard models [16, 17]. GCGM is based on the Gutzwiller wave function (GWF) proposed by Gutzwiller in 1960s [18, 19]. GWF uses a Jastrow-type correlator [20] which introduces the correlation effects by acting a projector $\hat{P}_G$ onto a single-particle product state: $|\Psi_G\rangle = \hat{P}_G|\Phi_0\rangle$. $\hat{P}_G$ projects $|\Phi_0\rangle$ onto the products of atomic configurations and modifies the weight of each atomic configuration based on the electronic occupation on the atom [21]. In the Gutzwiller correlator, each atom is modified independently; thus no site-site correlations are taken account of. The evaluation of GWF is in itself a difficult task, which often involves the Gutzwiller Approximation (GA). It has been demonstrated that GA introduces inaccuracies in a number of systems [22, 23]. In addition, GCGM incorporates site-site correlations that are missing in the pure GWF.

While the above-mentioned methods have documented a wide range of success on the ground state (GS), their generalization to target excited states (ES) remain a challenging task. For instance, the vibrational DMRG algorithm faces a major difficulty in finding an algorithm suitable for parallelization since the optimization of excited states starts from a ground-state search in the space orthogonal to the already optimized lower-lying wave functions [24]. Although growing efforts [25, 26] have been devoted to overcome this limitation, there still lacks an efficient technique for the calculations of excited states. The GCGM approach is easily parallelizable, but the performance of Gutzwiller-like projectors on excited states still needs to be fully examined.

In this work, we apply a generalized non-local Gutzwiller projector following the formalism proposed by Kaplan *et al.* [27] onto a series of eigenstates of a non-interacting system. The resulting GWFs span a manifold with controllable dimensionality. Exact diagonalization is then performed in this manifold to check whether it can reasonably

capture the ground and excited states of the true correlated system. We call this approach the extended Gutzwiller (EG) method. We report the initial benchmark results of the EG method on even-numbered Hubbard rings, whose exact solutions are readily available using ED techniques.

This article is organized as follows. In Sec. II, we give a detailed description of the EG method. Section III compares the results obtained by the EG and ED methods for the 10-site ($N = 10$) Hubbard ring at half-filling, including the wave function overlap (fidelity), the ground- and excited-state energy, double occupancy, the staggered magnetization, and the total spin. Furthermore, we test the EG method on dynamical properties by evaluating the electron-removal spectral functions. Conclusions and outlook are presented in Sec. IV.

2. Computational Methods

2.1. Non-local Gutzwiller projector

The original Gutzwiller wavefunction is constructed by applying a Gutzwiller projector $g^{\hat{D}}$ onto a non-interacting wavefunction Φ_0:

$$|\Phi_G\rangle = g^{\hat{D}}|\Phi_0\rangle, \tag{1}$$

where $\hat{D} = \sum_i \hat{n}_{i\uparrow}\hat{n}_{i\downarrow}$, is an operator counting the number of doubly occupied sites, and $|\Phi_0\rangle$ is usually a single Slater determinant

$$|\Phi_0\rangle = \prod_{k\sigma} \hat{c}^\dagger_{k\sigma}|\emptyset\rangle, \tag{2}$$

where $\hat{c}^\dagger_{k\sigma}$ creates a Bloch state with momentum k and spin σ. The product in Eq. 2 runs through all occupied Bloch states.

$|\Phi_0\rangle$ can be expanded based on a basis configuration as

$$|\Phi_0\rangle = \sum_\Gamma \lambda_\Gamma|\Gamma\rangle, \tag{3}$$

where

$$|\Gamma\rangle = \prod_{j\sigma} c^\dagger_{j\sigma}|\emptyset\rangle. \tag{4}$$

$c^\dagger_{j\sigma}$ creates a local electron at site j with spin σ. The product in Eq. 4 runs through all occupied local orbitals in $|\Gamma\rangle$. The creation operator $c^\dagger_{k\sigma}$ in the momentum space (see Eq. 2) and the creation operator $c^\dagger_{j\sigma}$ in the real space (see Eq. 4) are related by a Fourier transform

$$\hat{c}^\dagger_{k\sigma} = \frac{1}{\sqrt{N}} \sum_j e^{ikj} \hat{c}^\dagger_{j\sigma}. \tag{5}$$

Every basis configuration $|\Gamma\rangle$ is naturally an eigenstate of $\hat{D}$: $\hat{D}|\Gamma\rangle = n_d|\Gamma\rangle$, with n_d being the number of doubly occupied sites in $|\Gamma\rangle$. Thus, Eq. 1 can be re-written as

$$|\Phi_G\rangle = \sum_\Gamma g^{n_d}\lambda_\Gamma|\Gamma\rangle. \tag{6}$$

However, it is well-known that the pure Gutzwiller wavefunction is a poor approximation of the true ground-state wavefunction. The essential source of error is that the Gutzwiller projector in Eq. 1 is completely local without taking into account any inter-site correlations. To remedy this situation, Kaplan *et al.* introduced an additional projector $\hat{Q}$ that counts the the number of doubly occupied sites without an empty neighbor, effectively addressing the correlation between doubly-occupied and empty sites [27]. Here, we follow the same strategy while use slightly different formalism. In particular, we separate n_d into two parts: $n_d = n_d^p + n_d^{\tilde{p}}$, where n_d^p and $n_d^{\tilde{p}}$ denote the number of doubly-occupied sites with and without an empty nearest neighbor, respectively. For example, the sequence $|\cdots, \uparrow, \uparrow\downarrow, \emptyset, \uparrow\downarrow, \downarrow, \cdots\rangle$ can give an n_d^p of one or two depending on whether the empty site is allowed to be shared. We performed a numerical test on the ground state for the half-filled ring with $N = 10$ at $U = 5t$. n_d^p defined not allowing empty sites to be shared gives a slightly lower ground-state energy of about $3 \times 10^{-4}t$/site. Hence, we choose this definition of n_d^p for all the calculations. Then, we define the extended Gutzwiller (EG) wavefunction as

$$|\Phi_{EG}\rangle = \sum_{\Gamma} g_1^{n_d^p} g_2^{n_d^{\tilde{p}}} \lambda_\Gamma |\Gamma\rangle. \tag{7}$$

The parameters g_1 and g_2 are optimized to give the lowest variational energy of the full Hamiltonian. The original Gutzwiller wavefunction is recovered if the two variational parameters g_1 and g_2 are set to be equal. Here, to compare with ED results on a relatively small system, the EG wavefunction given in Eq. 7 is exactly evaluated by enumerating all possible configurations $|\Gamma\rangle$.

2.2. Manifold construction

Traditionally the Gutzwiller variational method was mainly implemented on the ground state. Here, we extend the EG method to study the excited states. To do so, we first choose the first M many-body eigen-wavefunctions of the non-interacting Hamiltonian as the initial wavefunctions. $|\Phi_0^{(i)}\rangle$ $(i = 0, 1, \cdots, M-1)$. For $|\Phi_0^{(0)}\rangle$, only the lowest-energy states $|k\sigma\rangle$ are occupied according to Eq. 2. For $i > 0$, higher-energy Bloch states are systematically introduced to replace the lower energy ones. Then, an EG wavefunction $|\Phi_{EG}^{(i)}\rangle$ is computed for each $|\Phi_0^{(i)}\rangle$ using the method described above. Since $|\Phi_{EG}^{(i)}\rangle$ are independent of each other, this process can be trivially parallelized. The M EG wavefunctions $|\Phi_{EG}^{(i)}\rangle$ are used as a basis to construct a subspace, which we term as the manifold. Finally, we diagonalize the Hamiltonian in this manifold to obtain the approximate ground and low-lying excited states. Since $|\Phi_{EG}^{(i)}\rangle$ are in general not orthogonal, the Hamiltonian $\hat{H}$ is diagonalized in the manifold by solving the following generalized eigenvalue problem:

$$\mathbf{Hu} = \epsilon \mathbf{Su}, \tag{8}$$

The interaction matrix $\mathbf{H}$ is defined by

$$\mathbf{H}_{ij} = \langle \Phi_{EG}^{(i)} | \hat{H} | \Phi_{EG}^{(j)} \rangle, \tag{9}$$

and the overlap matrix $\mathbf{S}$ is defined by

$$\mathbf{S}_{ij} = \langle \Phi_{EG}^{(i)} | \Phi_{EG}^{(j)} \rangle. \tag{10}$$

ϵ is the energy, and the vector $\mathbf{u}$ gives the approximate eigenstate of the Hamiltonian:

$$|\Psi_{EG}^{(i)}\rangle = \sum_{i=1}^{M} \mathbf{u}_i |\Phi_{EG}^{(i)}\rangle. \tag{11}$$

In Appendix A, we will show that $\mathbf{H}_{ij}$ and $\mathbf{S}_{ij}$ are non-zero only if the total momentums for $|\Phi_0^{(i)}\rangle$ and $|\Phi_0^{(j)}\rangle$ are differed by a multiple of 2π. In other words, $\mathbf{H}$ and $\mathbf{S}$ in Eq. 8 are already block diagonal; thus, the diagonalization of $\mathbf{H}$ and $\mathbf{S}$ matrices can be efficiently done for each block independently. In practice, we include M_b states in each block.

3. Results and discussions

3.1. Model

To illustrate the accuracy of the EG method, the half-filled Hubbard rings, where exact benchmark results are accessible from the exact diagonalization, are considered. The Hamiltonian is defined as follows:

$$\hat{H} = -t \sum_{\langle i,j \rangle, \sigma} \hat{c}_{i\sigma}^{\dagger} \hat{c}_{j\sigma} + U \sum_{i} \hat{n}_{i\uparrow} \hat{n}_{i\downarrow} \tag{12}$$

where $\hat{c}_{i\sigma}^{\dagger}(\hat{c}_{i\sigma})$ creates (annihilates) an electron at site i with spin σ, and $\hat{n}_{i\sigma} = \hat{c}_{i\sigma}^{\dagger}\hat{c}_{i\sigma}$. The first term represents the kinetic energy, only nearest-neighbor hopping is considered. The second term is the on-site Coulomb repulsion strength in proportion to the on-site interaction U. We have examined various physical quantities using the EG method and compared with the ED solutions, as will be discussed in detail in the following.

3.2. Energy spectra

We first discuss the exact solutions obtained by ED as implemented in Quanty, a script language for quantum many-body calculations [28]. Since energy levels commonly cross as U increases, we found it helpful to categorize the eigenstates based on the irreducible representation of the point group for the ring, as well as the total spin S. Each spin- and symmetry-resolved energy level extends as a smooth function of U. Here, we only consider even-numbered rings with periodic boundary conditions. Our ultimate goal is to develop an efficient method for an infinite lattice; that is, N is large enough that the thermodynamic limit behavior is approached. It is shown that under perfect periodic boundary condition, the odevity of the number of lattice sites, N, plays an unexpected role even in the thermodynamic limit. While systems with $N(\in odd) \to \infty$ suffer a ring frustration and exhibit a low-energy gapless spectrum above the ground state, systems with $N(\in even) \to \infty$ are free from the ring frustration problem [29,30] . Thus, we only

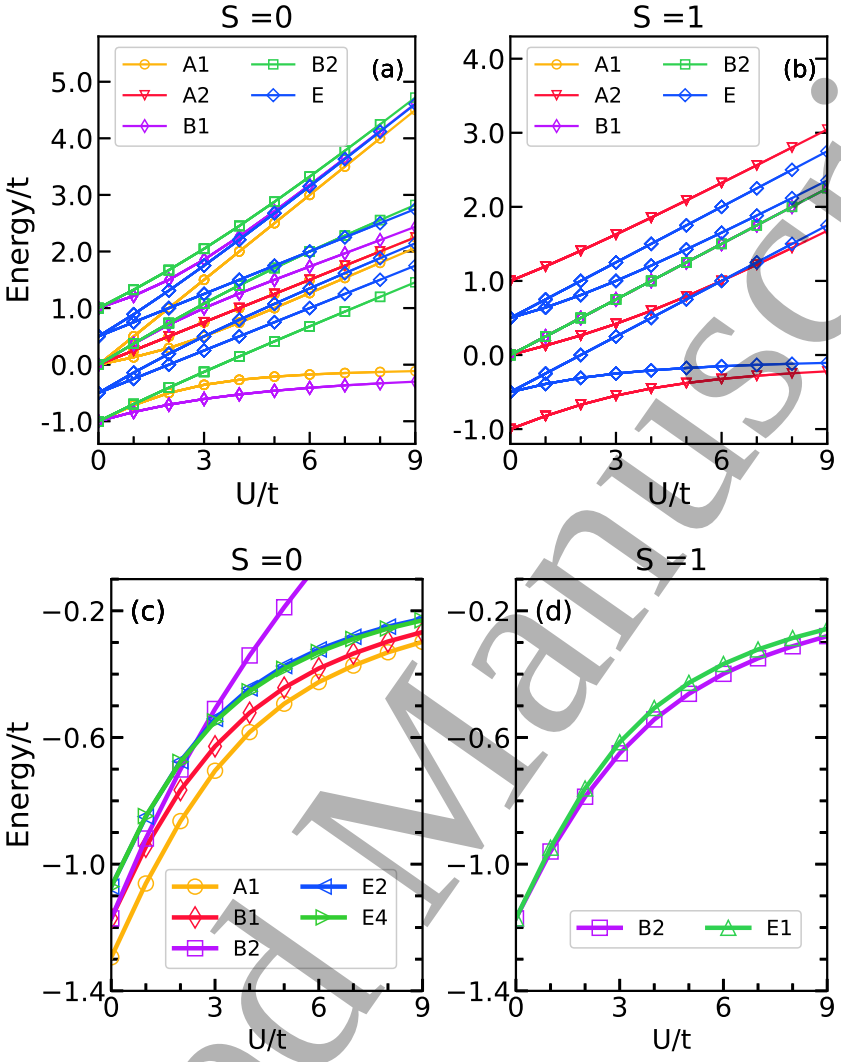

Figure 1. (a-b) Exact energy spectra as function of U/t for $N = 4$ Hubbard ring; (c-d) corresponding ones for $N = 10$. S denotes the total spin. We assigned point group symmetry representations ($A1$, $A2$, $B1$, $B2$, *et al.*) for the GS and ES wavefunctions of the $N = 4$ and $N = 10$ Hubbard rings in the light of the character tables of point groups C_{4v} and C_{10v}, respectively. The corresponding character tables are shown in Appendix B and can be found in ref [31].

focus on Hubbard rings with even number to deliver a proof-of-principle demonstration of our approach while avoiding the complications caused by other situations such as odd-numbered rings or open boundary conditions.

Figure 1 gives the exact energy spectra for $N = 4$ and $N = 10$ Hubbard rings. By examining their wavefunctions, we note that the group with higher energies contains larger number of doubly-occupied sites. For $N = 4$, in the limiting situation of $U \to \infty$, the three groups (from bottom to top) contain exactly 0, 1 and 2 doubly-occupied sites, respectively. The same energy separation behavior was reported by Viefers *et al.* in an early paper [32]. For $N = 4$, we showed all but a single eigenstate with $S = 2$ in

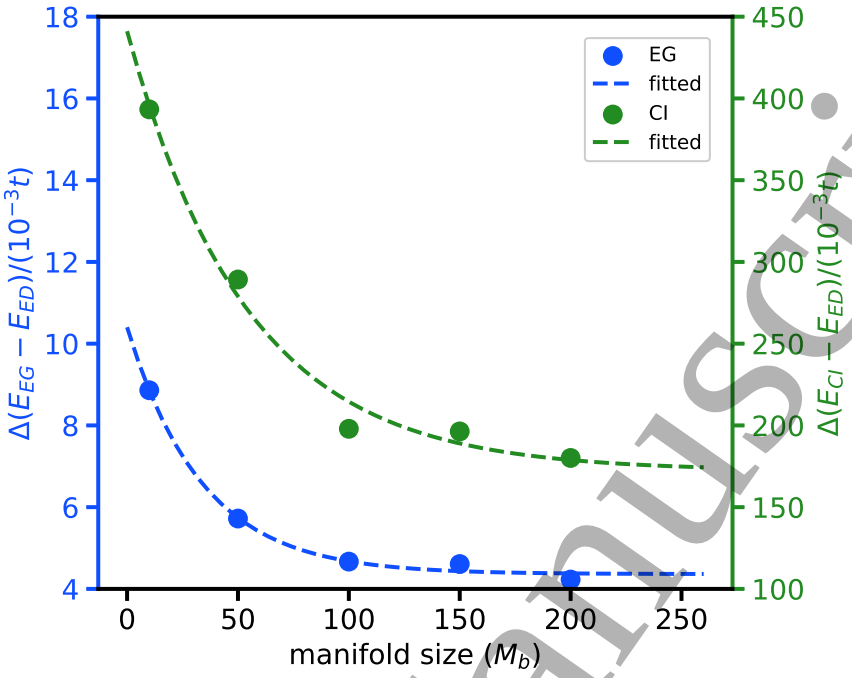

Figure 2. The ground state energy difference between the ED and the EG/CI methods for the half-filled 10-site Hubbard ring at $U/t = 5$.

figure 1(a-b). This corresponds to the ferromagnetic state, in which there is no doubly-occupied sites and the hopping is not allowed, giving a total energy of 0.

Similarly, we categorize the energy spectra of the $N = 10$ ring according to the symmetry and the total spin, as shown in figure 1(c-d). At large U, the eigenstates also separate into different groups based on the number of doubly-occupied sites. Here, we only show a few low energy states for simplicity. The ground state is a spin singlet ($S = 0$) with A_1 symmetry for any U. The first excited state belongs to the B_2 symmetry with $S = 1$. When $U/t < 2$, the second excited state is doubly-degenerate with E_1 symmetry and $S = 1$; and the third excited state is a singlet B_1 state with $S = 0$. At $U/t \geq 2$, the second state and the third state are inverted.

In the following, We use the $N = 10$ Hubbard ring as a prototype to examine the EG method in predicting the energy of the ground and excited states of a correlated system. To check the convergence of the manifold size M_b, we plot in Figure 2 the ground state energy difference between the ED and the EG methods as a function of the block size M_b at an intermediate $U/t = 5$. The dashed line is a fitting to the exponential decay function $\Delta E = \alpha e^{-\beta M}$ as a guide of eye. It is shown that when $M_b \sim 200$, the drop of the ground state energy becomes very small (on the order of $10^{-4}t$/site). Block sizes $M_b \leq 200$ were used in all the calculations reported in the manuscript.

The EG method can be considered as a generalization of the configuration interaction (CI) method in quantum chemistry. CI uses a variational wavefunction that is a linear combination of multiple configurations $\Psi = \sum_{i=0} c_i \Phi_i$, where Φ_0 is normally a

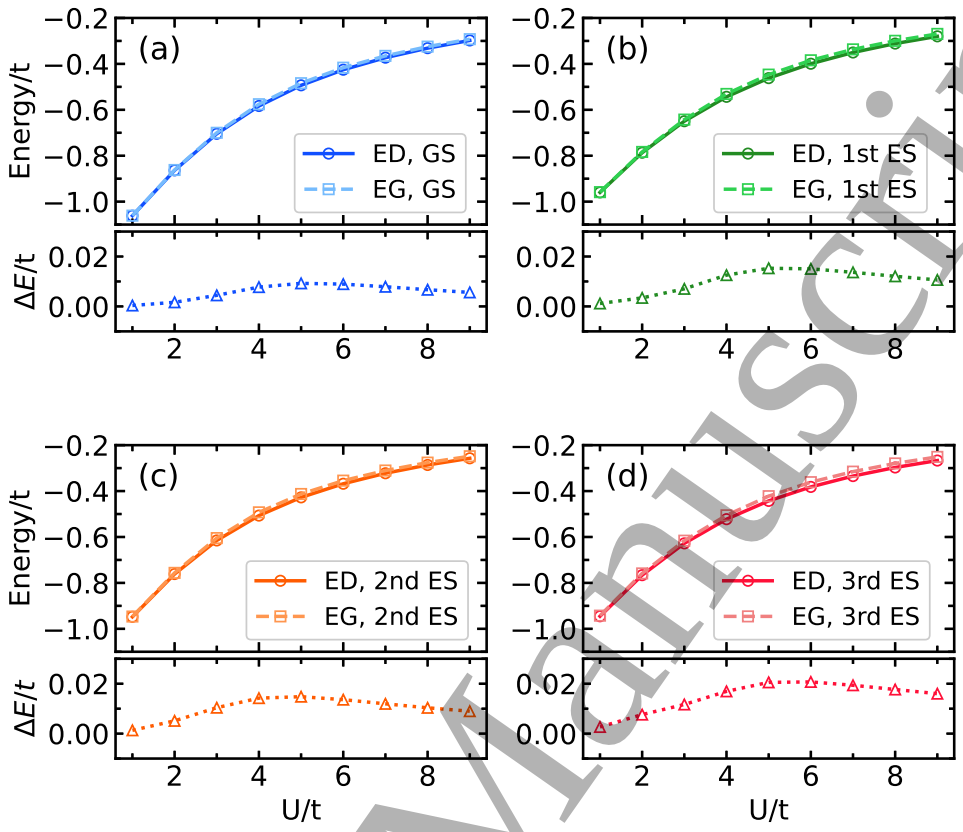

Figure 3. Ground state and excited state energies of $N = 10$ Hubbard ring as a function of U. Solid Lines with circles denote ED results, dashed lines with squares represent EG results, dotted lines with triangles are for absolute errors between two methods.

Hartree-Fock solution, and the successive Φ_i's are generated by hierarchical excitation of single-particle states resulted from mean-field calculations. c_i's are determined by diagonalization in the space spanned by Φ_i's. In CI, each Φ_i itself is non-correlated. In our approach, an EG projector is applied on Φ_i's before the construction of the manifold, thus profound correlations are already encoded in the basis wavefunctions. In Figure 2 , we also show the results for the CI method. Unlike the EG method, in which the manifold is spanned by the extended GWFs $|\Phi_{EG}^{(i)}\rangle$, in CI, the manifold is spanned by the non-correlated $|\Phi_0^{(i)}\rangle$. For the same M_b, the EG method gives a much better estimation of the ground-state energy than the CI method (note the different scales for the EG and CI energies). A similar approach has been applied in the quantum subspace expansion method for quantum computing, and has been demonstrated to help improve the ground state estimation, mitigate noise, and access a wide range of excited states [33].

Figure 3 shows the energy of the ground state and the first three excited state of the 10-site Hubbard ring as a function of U. The solid and dashed lines are for the ED and EG results, respectively. The absolute errors ($\Delta E = |E_{EG} - E_{ED}|$) are plotted in the

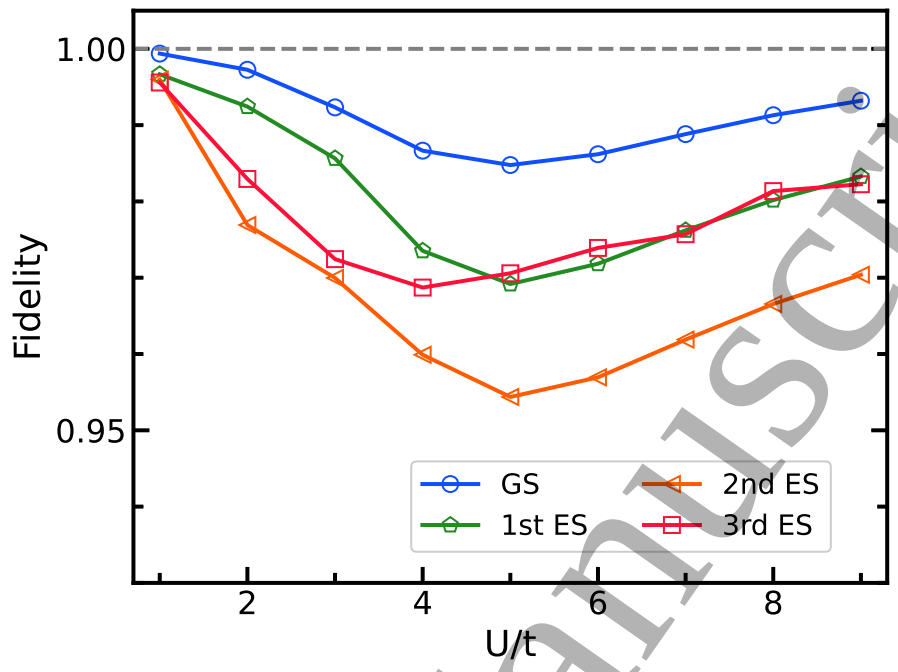

Figure 4. Fidelity of the GS and ES wavefunctions as a function of U.

bottom panel of each subplot. One can see that the EG results compare very favorably with the ED results. For the ground state, the deviations for all U/t values are within $0.01t$ per site. For excited states, the largest deviations, which are found around $U/t = 5$, reach $0.02t$ per site.

3.3. Fidelity

To examine the accuracy of the EG method in describing the GS and ES wave functions, we investigate the overlap between the exact GS/ES wave functions with those generated by the EG technique. The normalized wave function overlap (fidelity) is defined as

$$O_i = |\langle \Psi_{ED}^{(i)} | \Psi_{EG}^{(i)} \rangle|^2, \tag{13}$$

where $\Psi_{ED}^{(i)}$ and $\Psi_{EG}^{(i)}$ are the *ith* wavefunction calculated by the ED and the EG methods, respectively.

The fidelity as a function of U for the GS and the first three ES is presented in figure 4. Generally, the overlap is large at both ends of strong and week interactions, and reaches minimum at intermidiate $U/t \sim 5$. An overlap greater than 95% was observed for the entire U/t range, demonstrating the applicability of the EG method in producing reliable wave functions of the 1D Hubbard ring for both GS and ES.

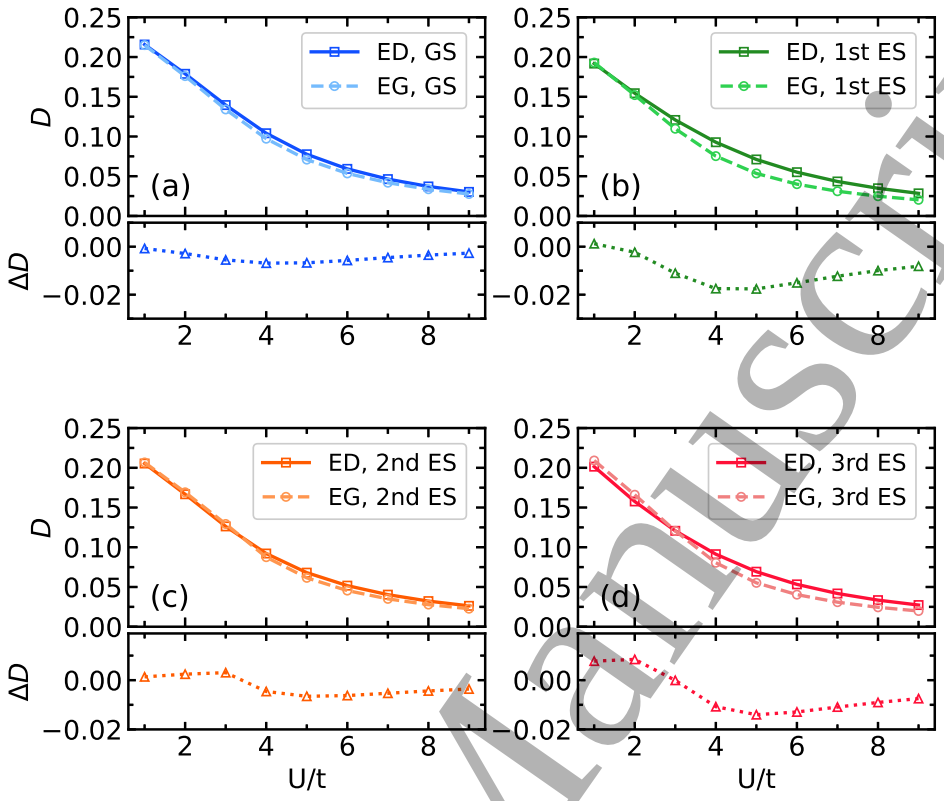

Figure 5. Comparison of double occupancy as a function of U for the $N = 10$ Hubbard ring at half-filling calculated by ED (solid lines) and by EG (dashed lines). ΔD denotes the difference between the two methods.

3.4. Observables

Based on the acquired wave functions, we can evaluate more physical quantities and compare with the ED results. These quantities include the double occupancy, the staggered magnetization and the total spin.

The double occupancy, which measures the derivative of energy with respect to U, provides useful insights into the correlation effects [34]. In figure 5, the double occupancy defined as $\langle \hat{D} \rangle / N$ is plotted as a function of U for GS and ES. Overall, the double occupancy calculated by the EG method agrees well with that obtained by the ED method, especially for ground state and the 2nd excited state. For the 1st and the 3rd excited states, some noticeble differences can be seen at intermediate U, consistent with the deviation of the wave functions in the same range (see figure 4).

The total spin S is a good quantum number since the total spin operator $\hat{S}^2$ commutes with the Hamiltonaian H. Here, we evaluate the expectation value of $\hat{S}^2$ with respect to the GS and ES obtained by the EG method to check the degree of spin contamination in the variational wavefunctions. Figure 6 depicts the $\langle \hat{S}^2 \rangle$ as a function of U for the $N = 10$ Hubbard ring. For the ground state, $\langle \hat{S}^2 \rangle$ exhibits slight deviations, which is about 0.25%, from the exact value of zero at $U/t > 4$. For the three

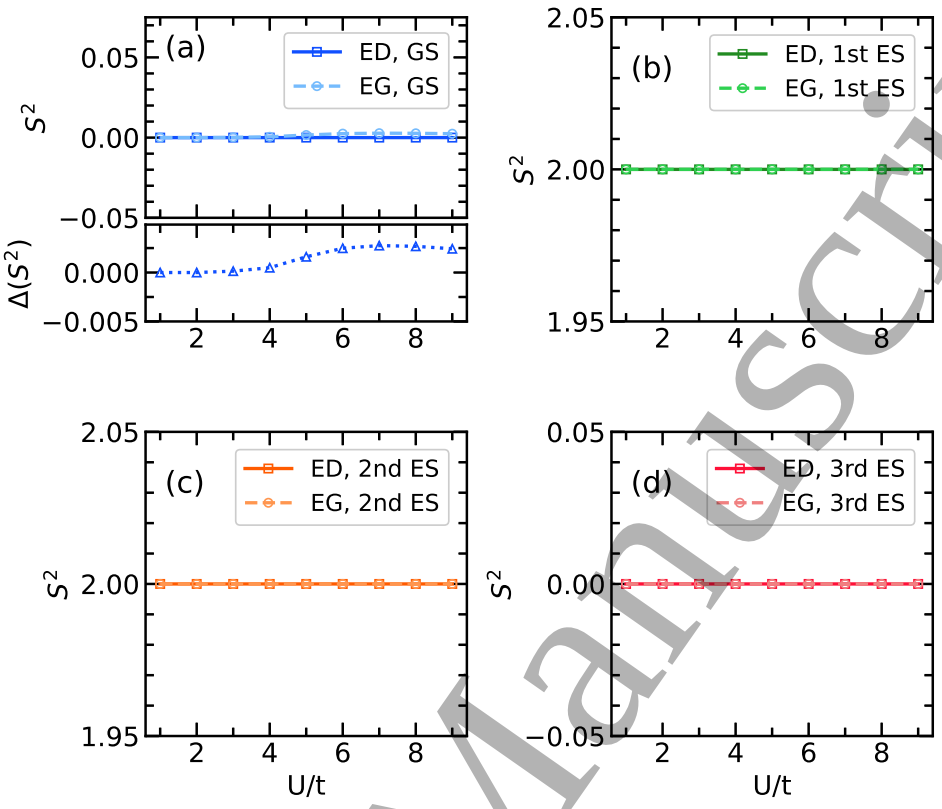

Figure 6. S^2 of ground state and excited states of $N = 10$ Hubbard ring as a function of U in comparison to ED results. Solid Lines with squares denote ED results, dashed lines with circles represent EG results. The lower panel of (a) shows the absolute errors between two methods for the ground state.

excited states, the EG method gives perfect values of the total spin, showing zero spin contamination for these excited states.

Staggered magnetization is often used as the order parameter to describe the antiferromagnetic order of a quantum many-body system. For the Hubbard ring, the staggered magnetization operator is defined as $\hat{\mathbf{m}} = \sum_{i=1}^{N} (-1)^i \hat{\mathbf{S}}_i / N$, where $\hat{\mathbf{S}}_i$ is the vector spin operator at site i. It is known that the ground state of a finite-size Hubbard ring at half-filling is a spin singlet, in which $\langle \hat{\mathbf{m}} \rangle$ vanishes due to the rotational symmetry. On the other hand, $\langle \hat{m}^2 \rangle = \langle \hat{m}_x^2 + \hat{m}_y^2 + \hat{m}_z^2 \rangle$ takes finite values, and its symptotic behavior at large N can reveal the antiferromagnetic order (or the lack thereof) in the thermodynamic limit. We show in figure 7 the ED and EG solutions of $\langle \hat{m}^2 \rangle$ as a function of U for ground state and the first three excite states. Again, the EG approach gives reasonable agreement with the ED method, especially for the ground state and the first two excite states, while some deviations are found for the third excite state.

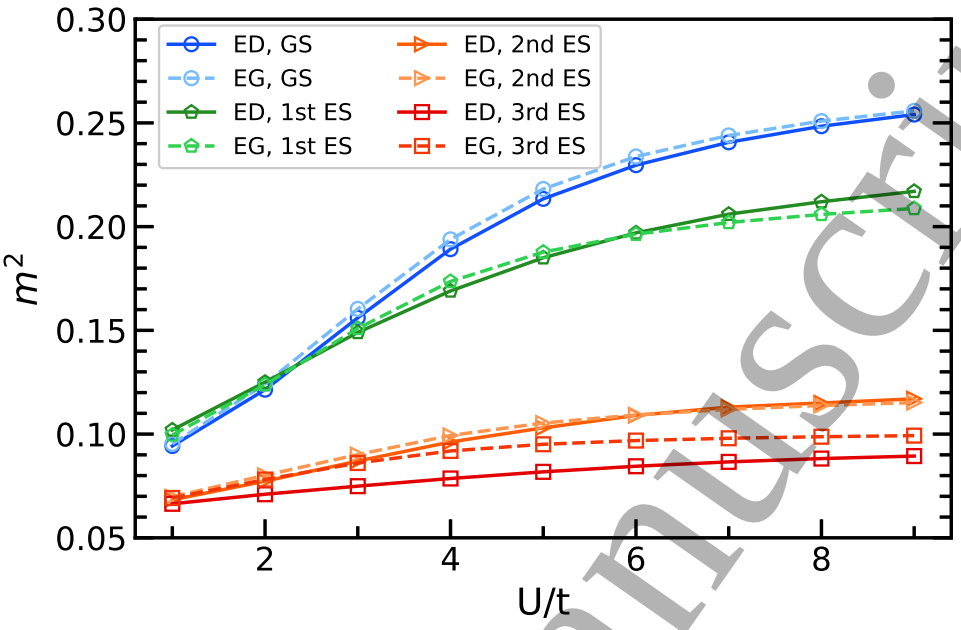

Figure 7. Squared sublattice magnetization $\langle m^2 \rangle$ of the ground state and excited states of $N = 10$ Hubbard ring at half-filling. Solid and dashed lines are for ED and EG solutions, respectively.

3.5. One particle spectral function

The experimental angular-resolved photoemission spectroscopy (ARPES) is a vastly successful method to probe the occupied electronic states for an interacting many-body solids. The photoelectron current in ARPES is directly proportional to the one-electron removal spectral function $A^-(k,\omega)$ [35], which precisely determines the probability of finding the quasiparticle resulted from the removal of a surface electron in a state with wave vector k and energy ω. Hence, the evaluation of $A^-(k,\omega)$ is essential for the interpretation of the measured ARPES spectra. The one-electron removal spectral function $A^-(k,\omega)$ is related to the imaginary part of the one-particle Green's function $G^-(k,\omega)$: $A^-(k,\omega) = -\frac{1}{\pi}\mathrm{Im}(G^-(k,\omega))$. $G^-(k,\omega)$ is defined as

$$\begin{aligned} G^-(k,\omega) &= \langle \Psi_0^N | \hat{c}_{k\sigma}^\dagger \frac{1}{\omega + (H - E_0^N) - i\eta} \hat{c}_{k\sigma} | \Psi_0^N \rangle \\ &= \sum_n |\langle \Psi_n^{N-1} | \hat{c}_{k,\sigma} | \Psi_0^N \rangle|^2 \frac{1}{\omega + (E_n^{N-1} - E_0^N) - i\eta}, \end{aligned} \tag{14}$$

where $|\Psi_0^N\rangle$ denotes the ground state of the N-number Hubbard ring at half filling (N electrons), with E_0^N being the corresponding ground-state energy. $|\Psi_n^{N-1}\rangle$ represents the nth eigensate of the N-number Hubbard ring with $N-1$ electrons. $\hat{c}_{k\sigma}^\dagger$ is related to the creators of local orbitals $\hat{c}_{j\sigma}^\dagger$ by a Fourier transform: $\hat{c}_{k\sigma}^\dagger = 1/\sqrt{N}\sum_j e^{ikj}\hat{c}_{j\sigma}^\dagger$. For the $N = 10$ ring, three k-points ($k = 0, \pi/5$, and $2\pi/5$) were used in the calculation. η is a Lorentzian broadening factor with a small value of 0.02. Both EG and ED methods

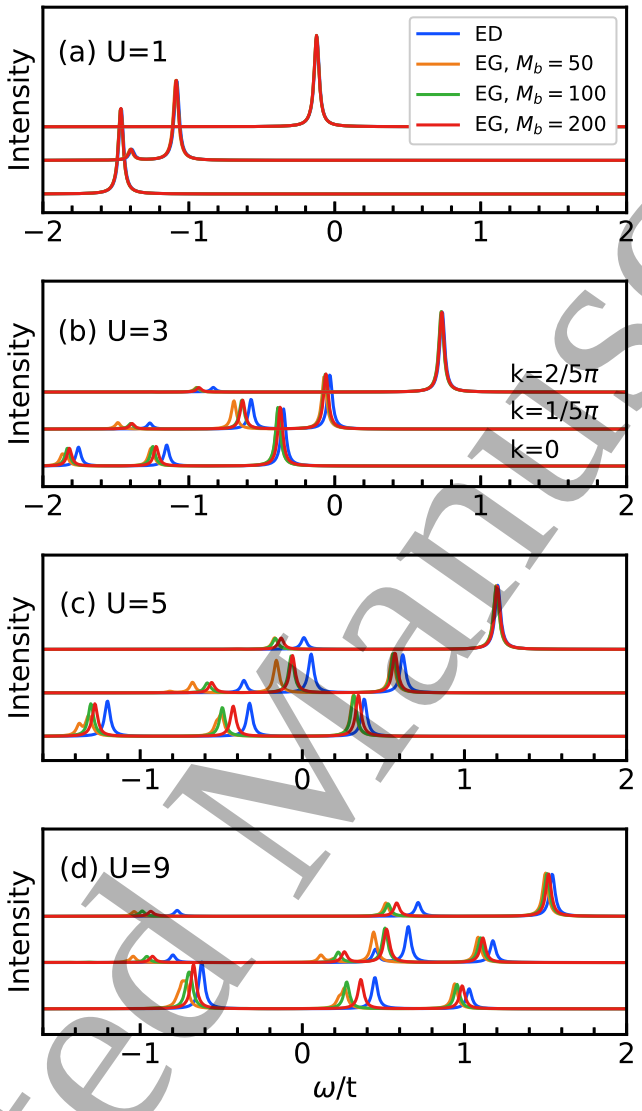

Figure 8. The k-resolved spectral functions of the $N = 10$ Hubbard ring at half-filling calculated with ED (blue lines) and EG (orange, green, and red lines for $M_b = 50$, 100, and 200, respectively) approaches. A broadening of 0.02 is used.

were applied for comparison purposes.

When $U = 0$, since $\hat{c}_{k\sigma}|\Psi_0^N\rangle$ is also an eigenstate of the Hamiltonian, there is only a single Lorentzian peak in the spectral function. However, at finite U, more states that satisfy momentum conservation can be excited upon removing one electron due to the correlation effects, giving rise to additional peaks in the spectral function. In figure 8, we show the spectral functions at several U. At $U/t = 1$, one can see a second peak emerges for $k = \pi/5$. The EG results agree very well with the ED ones in this case of weak interaction. More peaks can be seen as U increases. The peaks also shift in the right direction because the increase of the electronic chemical potential at stronger repulsive

interactions. It should be noted that the additional peaks are not contributed by the first several exited states of the $(N-1)$-electron system, but by states that are deep in the excited spectrum, as evidenced by the large energy separations between peaks. Nevertheless, the EG method can still capture these peaks with the relative strength comparing favorably with the ED method. There are noticeable shifts in the peak positions; however, these shifts remain relatively small compared with the separations between peaks. Overall, the EG method can capture the essential dynamical response in this correlated electron system.

Finally, we compare the computational cost for evaluating the spectral functions with EG and ED methods, using $k = 0$ at $U/t = 5$ as an example. To ensure a fair comparison, we performed the calculations with the same number of cores (i.e., 96 cores) for the two methods at their respective converged manifold size. It took 5.4h and 2.3h the ED and the EG method, respectively, to obtain the spectral functions. The comparison shows that the EG method appears to be more efficient. One should also note that in the current proof-of-principle demonstration, the matrices $\mathbf{H}$ and $\mathbf{S}$ as defined in Eq. 8 in the main text are evaluated exactly by enumerating all possible configurations (see Eq. A.6), which consumes most of the computer time. This process needs to be significantly sped up for larger systems, which is a focus of our current work.

4. Conclusion and outlook

We propose an extended Gutzwiller (EG) method to describe the ground and excited states for many-body systems with strong electron correlations. A generalized non-local Gutzwiller projector is applied onto the ground and excited states of a non-interacting system, followed by exact diagonalization in the manifold spanned by the resulting extended Gutzwiller wavefunctions. Using the $N = 10$ Hubbard ring as the benchmark system, we demonstrate that the EG method converges to the required accuracy much faster than the configuration interaction method since profound electron correlations have been encoded in the basis wavefunctions of the manifold. As a result, the EG method can reliably reproduce the ground and excited states of a strongly-correlated Hamiltonian. A series of physical quantities also compare favorably with the exact results, including energy, double occupancy, staggered magnetization and total spin. Furthermore, the EG method gives satisfactory electron-removal spectral functions, a quantity that plays an important role in interpreting the angle-resolved photoemission spectroscopy.

The main objective of the current study is to examine whether the EG method, which is a variational approach, can reach the required accuracy. For this reason, we chose a relatively small system ($N = 10$), whose exact solutions are available for comparison. The implementation of the EG method is also exact by enumerating all possible many-body configurations. Mature tools do exist in evaluating variational wavefunctions for large systems, such as the variational Monte Carlo (VMC) [36–38] or an alternative random-sampling method [39,40]. The GCGM method [14,15] represents

an even more efficient approach. The central part of these methods is to minimize the Rayleigh quotient [41], which corresponds to the diagonal terms of the matrices in Eq. 8. Two key challenges need to be addressed for these approaches to be applicable to the EG method. Firstly, we need to formulate an efficient way of evaluating the matrix elements $\mathbf{H}_{ij}$ and $\mathbf{S}_{ij}$, as defined in Eq. 8-10 for large systems. Secondly, we need to demonstrate that a no worse than polynomial scaling of the manifold size with the system size can be achieved, so that the method is tractable for large systems.

Acknowledgments

Work at Xiamen University was supported by the National Natural Science Foundation of China (No. 12147138 and No. 11874307) and the Fundamental Research Funds for the Central Universities of China (No. 20720210023). Work at Ames National Laboratory was supported by the US Department of Energy (DOE), Office of Science, Basic Energy Sciences, Materials Science and Engineering Division including a grant of computer time at the National Energy Research Scientific Computing Centre (NERSC) in Berkeley. Ames Laboratory is operated for the US DOE by Iowa State University under Contract No. DE-AC02-07CH11358. Work at Qingdao University was supported by the National Natural Science Foundation of China (No. 21773132).

Data availability statement

The data that support the findings of this study are available upon reasonable request from the authors.

Appendix A. Total momentum conservation in H and S matrices

Here, we prove that $\mathbf{H}_{ij}$ and $\mathbf{S}_{ij}$ as defined in Eqs. 9 and 10, respectively, are non-zero only if the total momentums for $|\Phi_0^{(i)}\rangle$ and $|\Phi_0^{(j)}\rangle$ are differed by a multiple of 2π. According to Eq. 2, we can write the Hartree-Fock solution as

$$|\Phi_0\rangle = |k_1\sigma_1, k_2\sigma_2, \cdots, k_{Ne}\sigma_{Ne}\rangle, \tag{A.1}$$

where Ne is the total number of electrons, and k_j and σ_j ($1 \leq j \leq N_e$) denote the momentum and spin for each occupied Bloch state, respectively. Each momentum can take values $2\pi j/N$ where j is an integer ranging from $-N/2$ to $N/2-1$. We use $k_{tot} \equiv \sum_{j=1}^{Ne} k_j$ to denote the total momentum for $|\Phi_0\rangle$. Similarly, each local configuration $|\Gamma\rangle$ can be written as

$$|\Gamma\rangle = |r_1\sigma_1', r_2\sigma_2', \cdots, r_{Ne}\sigma_{Ne}'\rangle, \tag{A.2}$$

where r_j and σ'_j are the position and spin for each occupied local orbital, respectively. The expansion coefficient λ_Γ in Eq. 3 can be calculated as a matrix determinant:

$$\lambda_\Gamma = \left(\frac{1}{\sqrt{N}}\right)^{Ne} \begin{vmatrix} e^{ik_1 r_1}\delta_{\sigma_1\sigma'_1} & e^{ik_1 r_2}\delta_{\sigma_1\sigma'_2} & \cdots & e^{ik_1 r_{Ne}}\delta_{\sigma_1\sigma'_{Ne}} \\ e^{ik_2 r_1}\delta_{\sigma_2\sigma'_1} & e^{ik_2 r_2}\delta_{\sigma_2\sigma'_2} & \cdots & e^{ik_2 r_{Ne}}\delta_{\sigma_2\sigma'_{Ne}} \\ \vdots & \vdots & \ddots & \vdots \\ e^{ik_{Ne} r_1}\delta_{\sigma_{Ne}\sigma'_1} & e^{ik_{Ne} r_2}\delta_{\sigma_{Ne}\sigma'_2} & \cdots & e^{ik_{Ne} r_{Ne}}\delta_{\sigma_{Ne}\sigma'_{Ne}} \end{vmatrix} \tag{A.3}$$

We use $|\Gamma + l\rangle$ to denote the configuration created by translating each orbital in $|\Gamma\rangle$ by l sites. That is,

$$|\Gamma + l\rangle \equiv |r_1 + l\ \sigma'_1, r_2 + l\ \sigma'_2, \cdots, r_{Ne} + l\ \sigma'_{Ne}\rangle, \tag{A.4}$$

Based on Eq. A.3, it is easy to verify that

$$\lambda_{\Gamma+l} = \prod_{j=1}^{Ne} e^{ik_j l}\lambda_\Gamma = e^{ik_{tot} l}\lambda_\Gamma \tag{A.5}$$

Now we consider the matrix element $\mathbf{H}_{ij}$. According to Eqs. 7 and 9,

$$\mathbf{H}_{ij} = \sum_{\Gamma,\Gamma'} G^{(i)}_{\Gamma'} G^{(j)}_{\Gamma} \lambda^{(i)*}_{\Gamma'} \lambda^{(j)}_{\Gamma} \langle\Gamma'|\hat{H}|\Gamma\rangle. \tag{A.6}$$

Here, for simplicity, we use G_Γ to denote the Gutzwiller projector acting on $|\Gamma\rangle$: $G_\Gamma = g_1^{n_d^p} g_2^{n_d^{\tilde{p}}}$ (see Eq. 7). Clearly, G_Γ is translation invariant: $G_\Gamma = G_{\Gamma+l}$ for any l. Due to the translational symmetry in the Hubbard ring, when (Γ, Γ') runs through the set of all possible configuration pairs in the summation in Eq. A.6, $(\Gamma + l, \Gamma' + l)$ runs through the same set. Therefore,

$$\mathbf{H}_{ij} = \frac{1}{N}\sum_{l=0}^{N-1}\sum_{\Gamma,\Gamma'} G^{(i)}_{\Gamma'+l} G^{(j)}_{\Gamma+l} \lambda^{(i)*}_{\Gamma'+l} \lambda^{(j)}_{\Gamma+l} \langle\Gamma' + l|\hat{H}|\Gamma + l\rangle \tag{A.7}$$

$$= \frac{1}{N}\sum_{\Gamma,\Gamma'} G^{(i)}_{\Gamma'} G^{(j)}_{\Gamma} \langle\Gamma'|\hat{H}|\Gamma\rangle \sum_{l=0}^{N-1} \lambda^{(i)*}_{\Gamma'+l} \lambda^{(j)}_{\Gamma+l} \tag{A.8}$$

$$= \frac{1}{N}\sum_{\Gamma,\Gamma'} G^{(i)}_{\Gamma'} G^{(j)}_{\Gamma} \lambda^{(i)*}_{\Gamma'} \lambda^{(j)}_{\Gamma} \langle\Gamma'|\hat{H}|\Gamma\rangle \sum_{l=0}^{N-1} \exp\left[i\left(k^{(j)}_{tot} - k^{(i)}_{tot}\right) l\right]. \tag{A.9}$$

In Eq. A.8, we have used the translation invariance of both the Gutzwiller projector G_Γ and the Hamiltonian $\hat{H}$ as defined in Eq.12. The sum of the phase factors in Eq. A.9 $\sum_{l=0}^{N-1} \exp\left[i\left(k^{(j)}_{tot} - k^{(i)}_{tot}\right) l\right] = N$ if $k^{(j)}_{tot} - k^{(i)}_{tot}$ is a multiple of 2π, or 0 otherwise since $N(k^{(j)}_{tot} - k^{(i)}_{tot})$ is always a multiple of 2π. This concludes the proof that $\mathbf{H}_{ij}$ is non-zero only if the total momentums for $|\Phi^{(i)}_0\rangle$ and $|\Phi^{(j)}_0\rangle$ are differed by a multiple of 2π. To prove the same property for $\mathbf{S}_{ij}$, one only needs to replace $\hat{H}$ with the identity in Eqs. A.6-A.9, which is also translation invariant.

Appendix B. Character table

Table B1. The character table for the C_{4v} point group.

C_{4v}	E	$2C_4(z)$	C_2	$2\sigma_v$	$2\sigma_d$
A_1	1	1	1	1	1
A_2	1	1	1	-1	-1
B_1	1	-1	1	1	-1
B_2	1	-1	1	-1	1
E	2	0	-2	0	0

Table B2. The character table for the C_{10v} point group.

C_{10v}	E	$2C_{10}$	$2C_5$	$2C_{10}^3$	$2C_5^2$	C_2	$5\sigma_v$	$5\sigma_d$
A_1	1	1	1	1	1	1	1	1
A_2	1	1	1	1	1	1	-1	-1
B_1	1	-1	1	-1	1	-1	1	-1
B_2	1	-1	1	-1	1	-1	-1	1
E_1	2	$2\cos(\pi/5)$	$2\cos(2\pi/5)$	$-2\cos(2\pi/5)$	$-2\cos(\pi/5)$	-2	0	0
E_2	2	$2\cos(2\pi/5)$	$-2\cos(\pi/5)$	$-2\cos(\pi/5)$	$2\cos(2\pi/5)$	2	0	0
E_3	2	$-2\cos(2\pi/5)$	$-2\cos(\pi/5)$	$2\cos(\pi/5)$	$2\cos(2\pi/5)$	-2	0	0
E_4	2	$-2\cos(\pi/5)$	$2\cos(2\pi/5)$	$2\cos(2\pi/5)$	$-2\cos(\pi/5)$	2	0	0

References

[1] Hubbard J 1963 *Proc. R. Soc. Lond. A Math. Phys. Sci.* **276** 238–257

[2] Kim C, Shen Z X, Motoyama N, Eisaki H, Uchida S, Tohyama T and Maekawa S 1997 *Phys. Rev. B* **56** 15589

[3] Zou Z and Anderson P 1988 *Phys. Rev. B* **37** 627

[4] Lieb E H and Wu F Y 1994 Absence of mott transition in an exact solution of the short-range, one-band model in one dimension *Exactly Solvable Models of Strongly Correlated Electrons* (World Scientific) pp 9–12

[5] Bannister R and d'Ambrumenil N 2000 *Phys. Rev. B* **61** 4651

[6] Rodríguez-Guzmán R, Schmid K, Jiménez-Hoyos C A and Scuseria G E 2012 *Phys. Rev. B* **85** 245130

[7] Sorella S, Tosatti E, Baroni S, Car R and Parrinello M 1988 *Int. J. Mod. Phys.* **2** 993–1003

[8] Imada M and Hatsugai Y 1989 *J. Phys. Soc. Japan.* **58** 3752–3780

[9] White S R 1992 *Phys. Rev. Lett.* **69** 2863

[10] Dukelsky J and Pittel S 2004 *Rep. Prog. Phys.* **67** 513

[11] Baiardi A and Reiher M 2020 *J. Chem. Phys.* **152** 040903

[12] Luttinger J M and Ward J C 1960 *Phys. Rev.* **118** 1417

[13] Potthoff M 2003 *Eur. Phys. J. B* **32** 429–436

[14] Ye Z, Yao Y X, Zhao X, Wang C Z and Ho K M 2019 *J. Phys. Condens. Matter.* **31** 335601

[15] Ye Z, Fang Y, Zhang H, Zhang F, Wu S, Lu W C, Yao Y X, Wang C Z and Ho K M 2022 *J. Phys. Condens. Matter.* **34** 243001

[16] Ye Z, Zhang F, Yao Y X, Wang C Z and Ho K M 2020 *Phys. Rev. B* **101** 1–11 ISSN 24699969

[17] Ye Z, Zhang F, Yao Y X, Wang C Z and Ho K M 2021 *Mol. Phys.* **119** e1797917

[18] Gutzwiller M C 1963 *Phys. Rev. Lett.* **10** 159

[19] Gutzwiller M C 1964 *Phys. Rev.* **134** A923

[20] Jastrow R 1955 *Phys. Rev.* **98** 1479
[21] Bünemann J, Weber W and Gebhard F 1998 *Phys. Rev. B* **57** 6896–6916
[22] Gutzwiller M C 1965 *Phys. Rev.* **137** A1726
[23] Metzner W and Vollhardt D 1988 *Phys. Rev. B* **37** 7382
[24] Baiardi A, Stein C J, Barone V and Reiher M 2017 *J. Chem. Theory Comput.* **13** 3764–3777
[25] Baiardi A, Stein C J, Barone V and Reiher M 2019 *J. Chem. Phys.* **150** 094113
[26] Baiardi A, Kelemen A K and Reiher M 2021 *J. Chem. Theory Comput.* **18** 415–430
[27] Kaplan T A, Horsch P and Fulde P 1982 *Phys. Rev. Lett.* **49** 889–892
[28] Lu Y, Höppner M, Gunnarsson O and Haverkort M 2014 *Phys. Rev. B* **90** 085102
[29] Dong J J, Li P and Chen Q H 2016 *J. Stat. Mech. Theory Exp.* **2016** 113102
[30] Boudreault C, Owerre S A and Paranjape M B 2023 *arXiv preprint arXiv:2302.10789*
[31] Gelessus A, Thiel W and Weber W 1995 *J. Chem. Educ.* **72** 505
[32] Viefers S, Koskinen P, Deo P S and Manninen M 2004 *Physica E Low Dimens. Syst.* **21** 1–35
[33] McClean J R, Kimchi-Schwartz M E, Carter J and de Jong W A 2017 *Phys. Rev. A* **95** 42308
[34] Kocharian A, Yang C and Chiang Y 1999 *Phys. Rev. B* **59** 7458
[35] Giuliani G and Vignale G 2005 *Quantum theory of the electron liquid* (Cambridge university press)
[36] Gros C 1989 *Ann. Phys.* **189** 53–88
[37] Eichenberger D and Baeriswyl D 2007 *Phys. Rev. B* **76** 180504
[38] Tocchio L F, Gros C, Zhang X F, Eggert S *et al.* 2014 *Phys. Rev. Lett.* **113** 246405
[39] Zhang F, Ye Z, Yao Y X, Wang C Z and Ho K M 2021 *Mol. Phys.* **119** e1812745
[40] Zhang F, Ye Z, Yao Y X, Wang C Z and Ho K M 2021 *J. Phys. Commun.* **5** 125003
[41] Helgaker T, Jorgensen P and Olsen J 2014 *Molecular electronic structure theory* (John Wiley & Sons)